Linear and Nonlinear Rheology of Dendritic Star Polymers: Experiment

Jung Hun Lee,*,† Katerina Orfanou,‡ Paraskevi Driva,‡ Hermis Iatrou,‡ Nikos Hadjichristidis,‡ and David J. Lohse†

ExxonMobil Research and Engineering Company, Annandale, New Jersey 08801, and Department of Chemistry, University of Athens, Panepistimiopolis Zografou, 15771 Athens, Greece

Received June 25, 2008; Revised Manuscript Received September 17, 2008

ABSTRACT: The stress relaxation dynamics of a series of second and third generation dendritic star polymers have been investigated experimentally in the linear regime with small amplitude oscillatory shear and also by nonlinear step shear deformations. In linear rheology, the relaxation dynamics of dendritic star melts agree with the expected relaxation hierarchy, where the characteristic tan(δ) minima that appear at high frequency correspond to the faster relaxing parts of the given dendritic topology. On the other hand, the degree of dilution, estimated from the ratio of the second plateau modulus G_{II} to the rubbery plateau modulus G_N, was much less than the expectation of the hierarchical theory, which implies a relatively slower rate of dilution due to multiple arms and generations. The nonlinear damping behavior of the second generation dendritic architecture was similar to that of H-shaped/multiarm architectures, featuring a novel damping transition from less strain softening to agreement with the Doi−Edwards damping function as the branch-point withdrawal motion. The third generation dendritic polymers exhibited much weaker strain dependence than second generation samples, suggesting a stronger stretching effect due to multiple branching generations even with arms of a few entanglements at each generation. Such a stretching effect even with small arms at each generation induced extensional hardening in the linear polymer matrix maintaining the shear viscosity.

1. Introduction

Progress in the development of hierarchical tube model theories has greatly advanced our general understanding of the relaxation dynamics of macromolecules with various branched architectures.[1−12] This is both an intriguing scientific question as well as a matter of large technological import. Long chain branching is found in a large fraction of the polymers that are made and used commercially, particularly in the largest class of synthetic macromolecules, polyolefins. This branching is often uncontrolled, and the producer of such polymers needs to balance the generally beneficial effects of the branching on the ease of processing and forming these materials with the ofttimes detrimental impact of mechanical behavior. If one could determine exactly how the details of the branching architecture control the flow of such polymers, it is likely that the improved balance of processability and performance could be achieved.

The basic tenet of the hierarchical relaxation mechanism is that the nature of the branching architecture imposes a hierarchy of relaxation steps on the molecule. Thus, the outer parts of the molecule (i.e., those segments with a free end) relax first, followed by the inner segments attached to the already relaxed parts, followed by the next level of segments, ands so on. So the entire molecule relaxes only after the last relaxation of innermost parts is completed. The key assumptions of the hierarchical tube model are (1) continuously increasing dilution of the entanglement network ("dynamic dilution"), wherein the effect of already relaxed portions of a branched polymer is represented as an effective solvent for the still unrelaxed portions at time scales longer than their relaxation time and (2) the motion of branch-point with additional frictional drag caused by already relaxed outer branches/arms, which is represented as the branch-point diffusivity $D_{bp} = \delta^2/(2\tau_a)$. Here, τ_a is the outer arm relaxation time and $\delta = (pa)$ is an unknown hopping distance of a branch-point with a normalized hopping barrier p and a given tube diameter a.[1,2] For example, the model of arm retractions followed by the reptative diffusion of linear-like backbone under the diluted network assumption has been very successful in predicting the stress relaxation behavior of H-shaped,[2,8] multiarm,[6,8,11] and comb polymers[4,6−11] beyond qualitative agreement.

In this viewpoint, the dendritic star structure that we examine herein is of specific interest as one of the simplest "branch-on-branch" architectures. As can be seen in Figure 1, these dendritic stars star with a single interior branch point, from which some number of arms extends. At the end of each arm is another, secondary branch point, from which more arms extend. At the end of these arms are the tertiary branch points, followed by arms. This continues through the generations of the dendritic star until finally the free ends are reached. An obvious merit of the dendritic star structure is that relaxation dynamics will be governed by only the arm retraction process, unlike H-shaped, multiarm, or comb polymers, which have chain segments along the linear-like backbone relaxing at the last hierarchal level. Also, the symmetrical nature of dendritic structures fixes the number of outer arms per branch-point and the number of branch-points per inner arm. Therefore, the linear viscoelasticity of dendritic star polymers is particularly enlightening for the investigation of the relaxation dynamics of "branch-on-branch" architectures.

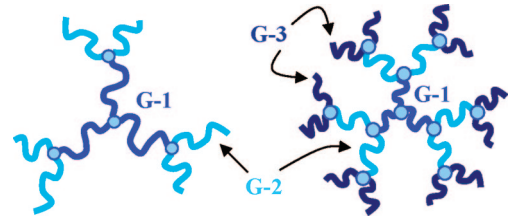

Figure 1. Schematic illustration of the second and third generation dendritic star polymers.

* To whom correspondence should be addressed. E-mail: menthol88@hotmail.com.
† ExxonMobil Research and Engineering Company.
‡ University of Athens.

10.1021/ma801429k CCC: $40.75
Published on Web 11/04/2008

Blackwell et al.[3] have recently proposed a theory for the linear and nonlinear rheology of a three-level Cayley-tree based on the hierarchical model framework. The authors imagined a third generation dendritic star architecture wherein all the arms were entangled. The center of this molecule was a symmetric three-arm star with all free ends of the first generation arms (G-1) linked to two second generation arms (G-2). Again the free end of each G-2 arm was linked to two third generation arms (G-3). Therefore, the total number of arms of type G-2 was six (via three branch-points) and that of G-3 arms was 12 (via six branch-points). The relaxation dynamics of this complex branched architecture was straightforwardly formulated as consecutive arm retraction process at each generation accounting for the variation in branch-point diffusivity. The stress in the nonlinear regime was calculated with the coupling effect between different generations on stretch and orientation dynamics, which was not considered in the previous H-shaped/multiarm model.[3] However, none of their predictions could be compared with any experimental data because well-defined model dendritic star polymers were not available at that time.

Recently, we have synthesized well-characterized, entangled second and third generation dendritic star (2GDS and 3GDS, respectively) polybutadienes using a novel anionic method.[13] Those dendritic polymers consist of a symmetric three-arm star at the center and two arms at each generation as Blackwell et al.[3] hypothetically envisioned. This means the rheological behavior of a simple "branch-on-branch" architecture has become experimentally accessible. More recently, van Ruymbeke et al. studied the linear viscoelasticity of these second and third generation dendritic polybutadiene melts and solutions.[12] The authors observed that the degree of dilution, evaluated by the ratio of the second plateau modulus G_{II} to the rubbery plateau modulus G_N, became weaker as the fraction of unrelaxed inner portions decreased. Also, a general tube-based model with a time-marching algorithm was proposed to predict the relaxation dynamics with the dilution exponent α and the normalized hopping parameter p fixed as 1. A distinctive assumption in their approach is the equilibrium contour length of just relaxed outer arms was nonzero, so that already relaxed portions of a dendritic star (e.g., the outer arms in 2GDS structures) are still involved in the relaxation of the unrelaxed portions (e.g., the inner arms in 2GDS) as a part of the effective contour length of inner arms.[12] The effective contour length as a sum of inner and outer arms leads to the relaxation of inner arm beginning at a nonzero fractional distance $s^* = M_{inner}/(M_{inner} + M_{outer})$, where M_{inner} and M_{outer} are the molecular weights of the inner and outer arm, respectively. In the hierarchical theories, however, the relaxation of inner arm starts from a zero fractional distance $s = 0$ because the outer arms are regarded as an effective solvent after their relaxation time $\tau_{outer}(s = 1)$. It is noteworthy that the onset of inner arm relaxation at either a zero or a nonzero fractional distance causes a time-discontinuity at the branch-point. That is, $\tau_{inner}(s^* = \text{nonzero})$ becomes much slower than $\tau_{outer}(1)$, while $\tau_{inner}(s = \text{zero})$ becomes much faster. To maintain the time-continuity at the branch-point, Blackwell et al.[3] suggested a simple addition of $\tau_{outer}(1)$ to the inner arm relaxation time as a waiting time. On the other hand, van Ruymbeke et al.[12] made the onset time of inner arm relaxation equal to $\tau_{outer}(1)$ by introducing a renormalized molecular weight $M_{inner} + M_{G^*}$, which determines the effective contour length and the terminal relaxation dynamics of inner arms.

In this article, we report on the rheological features characteristic of polymers with dendritic architecture. The linear rheology of two kinds of dendritic stars, one using polybutadiene and the other polyisoprene, were measured and are used to illustrate the general characteristics of their stress relaxation behavior. The obtained experimental data is used to evaluate the capability of the hierarchical theory to predict linear viscoelasticity of "branch-on-branch" architectures. As mentioned above, the symmetrical nature of dendritic topologies fixes the number of arms per branch-point and the number of branch-points per arm. Thus, the only undetermined model parameters are the dilution exponent α, an unknown hopping barrier parameter p, the rubbery plateau modulus G_N, the entanglement molecular weight M_e, and the entanglement relaxation time τ_e. Blackwell et al.[3] expected that the dilution effect with $\alpha = 4/3$ would become dominant in dendritic architectures as relaxation proceeds, while in the model of Ruymbeke et al.,[12] the renormalized but increased entanglement densities of the inner arms with $\alpha = 1$ were needed to predict linear viscoelasticity. Rather than modify these mechanisms or add any new ones, in this paper we investigate which parameter can effectively remedy any observed discrepancies between predictions and experiments. In other words, we compare the predictions (with possible adjustable parameters but given arm molecular weights) to provide an insight into which model parameters or relaxation mechanisms are responsible for discrepancies between theory and experiment.

In terms of the nonlinear rheology, we focus on the shear relaxation modulus $G(\gamma,t)$ following the imposition of step strains to understand the effect of dendritic topology on the degree of chain stretching. The damping function $h(\gamma)$ is quantified as $h(\gamma) = G(\gamma,t)/G(t)$, where the equilibrium modulus $G(t)$ is $G(\gamma,t)$ at $\gamma \ll 1$.[14,15] In most cases the experimental values of $h(\gamma)$ for linear polymers with weak to moderate entanglement densities is in good agreement with the universal damping function of the Doi−Edwards tube model theory, h_{DE}.[14] This type of damping is generally categorized as type A behavior.[15] Highly entangled polymer melts, however, show a stronger strain dependence (called type C), exhibiting a damping function below the universal damping h_{DE}. On the other hand, branched polymers such as low density polyethylene exhibit a weaker strain dependence (type B) and show a damping function above the universal damping h_{DE}.[15] For polymers with a dendritic architecture, the inner arms trapped between two branch-points are expected to be stretched gradually according to applied strains. Once a degree of stretching of an inner arm reaches a critical limit, the tension to maintain its equilibrium contour length becomes large enough to pull the branch-point into the inner arm tube.[2,3,16,17] This pulling motion, named the branch-point withdrawal, was theoretically suggested a decade ago in H-shaped architectures,[16] while Archer et al.[18,19] experimentally observed the branch-point withdrawal motion as a novel transition in damping behavior from type B to h_{DE} beyond a certain strain using multiarm polybutadiene polymers. Thus, the damping functions of dendritic stars are of interest to evaluate the effect of dendritic topology as well as the physical picture of the branch-point withdrawal.

2. Experimental Section

2.1. Materials. A series of well-characterized second and third generation dendritic star polybutadienes (2GDSPBD and 3GDSPBD) and second generation dendritic star polyisoprenes (2GDSPI) were synthesized by a novel anionic method using 4-(dichloromethylsilyl)-diphenylethylene (DCMSDPE) linkers under high vacuum. Details of the synthesis procedure were described in a recent paper.[13] Briefly, the synthesis steps were the following: (a) selective reaction of living chains with the two chlorosilane group of DCMSDPE to produce a double-tailed DPE (dtDPE), which was not a homopolymerizable monomer; (b) addition of *s*-BuLi to the double bond in DPE group of the dtDPE to create a new anionic site; (c) polymerization of the appropriate monomer from the newly created anionic site to make living star dendrons; and (d) reaction of the produced living star dendrons with trichloromethyl silane to make the final second generation dendritic stars (2GDS). Molecular

Table 1. Molecular Characteristics of Dendritic Star Melts

sample name	$M_{w,G\text{-}1}$ [kg/mol]	$M_{w,G\text{-}2}$ [kg/mol]	$M_{w,G\text{-}3}$ [kg/mol]	$\omega_{crossover}$ [rad/sec]	$\omega_{\eta''max}$ [rad/sec]	G_{II}/G_N
2GDSPI G(18,29)	29.7	18.5		3.835×10^{-2}	1.995×10^{-2}	0.256
2GDSPI G(18,46)	46.5	18.5		4.002×10^{-3}	1.580×10^{-3}	0.360
2GDSPBD G(14,12)	12.2	14.3		6.474×10^{-2}	3.981×10^{-2}	0.0811
2GDSPBD G(19,23)	23.2	19		7.865×10^{-5}		0.131
3GDSPBD G(5,6,5)	5.4	5.8	4.7	5.405	5.623×10^{-1}	0.297
3GDSPBD G(5,6,32)	32.2	6.1	4.7	4.466×10^{-3}		0.415
3GDSPBD G(14,15,1)	1.1	15	13.8	2.308×10^{-3}		0.155

weights of the intermediates and final products at each synthesis step were characterized by a size exclusion chromatography with two angle laser light scattering (SEC-TALLS). Dendritic architectures are illustrated in Figure 1 and molecular characteristics of all dendritic star polymers are provided in Table 1. The molecular weight of the outer arm ($M_{w,G\text{-}2}$) of 2GDS was directly measured using the living chains synthesized in step (a), while the molecular weight of the inner arm ($M_{w,G\text{-}1}$) was calculated by subtracting two times of $M_{w,G\text{-}2}$ from the molecular weight of the living star dendrons made in step (c). For example, the reliability of the inner arm molecular weight and the degree of structural heterogeneity could be indirectly examined by comparing two values of $M_{w,G\text{-}1}$ of 2GDSPI G(18,46) from the molecular weights of the intermediate star dendron ($M_{w,dend} = 83.5$ kg/mol with $M_w/M_n = 1.04$) and the final product ($M_{w,total} = 250$ kg/mol with $M_w/M_n = 1.08$). The value of $M_{w,G\text{-}1}$ by subtracting two times of $M_{w,G\text{-}2}$ (= 18.5 kg/mol) from $M_{w,dend}$ is 46.5 kg/mol, while $M_{w,G\text{-}1} = 46.3$ kg/mol is obtained from the $M_{w,total}$ (i.e., $M_{w,G\text{-}1} = [M_{w,total} - 6 \times M_{w,G\text{-}2}]/3$). These values of $M_{w,G\text{-}1}$ also reflect the structural homogeneity of current polymers.

2.2. Rheological Measurements. Stress relaxation dynamics were quantified using small amplitude oscillatory shear measurements. A Rheometrics Scientific Inc. (RSI) ARES-LS rheometer with 6 mm or 10 mm diameter parallel-plate fixtures was used for all experiments in linear regime. Dynamic storage and loss moduli, $G'(\omega)$and $G''(\omega)$, of dendritic stars were measured at temperatures ranging from −80 to 28 °C. The Orchestrator software was used to generate master curves at a reference temperature $T_{ref} = 28$ °C by a two-dimensional residual minimization method. The WLF fit for the shift a_T, $\log(a_T) = [-C_1(T-T_{ref})]/[C_2 + T - T_{ref}]$, yields $C_1 = 5.1$ (± 0.5) and $C_2 = 143$ (± 7) °C for dendritic polyisoprenes and $C_1 = 4.5$ (± 0.8) and $C_2 = 184$ (± 18) °C for dendritic polybutadienes.

The nonlinear relaxation modulus $G(\gamma,t)$ after the imposition of step strains was measured using an Anton Paar Physica Modular Compact Rheometer (MCR501) with a 10 mm diameter cone-and-plate (angle 2°) fixture at 28 °C. To ensure complete relaxation between sequential step shear experiments, each measurement was made over a period more than 100 times the evaluated terminal relaxation time $\tau_{\eta''} = 1/\omega_{\eta''}$. This frequency, $\omega_{\eta''}$, is that at which $\eta''(\omega) \equiv G'(\omega)/\omega$ manifests a local maximum. For example, one measurement after imposition of a step deformation takes 6010 s for 2GDSPI G(18,29) for which $\tau_{\eta''}$ is 50 s. The damping function, $h(\gamma) = G(\gamma,t)/G(t)$, was quantified using the relaxation modulus $G(\gamma,t)$ at $\gamma = 0.1$ as the equilibrium modulus $G(t)$.

3. Results and Discussion

3.1. Linear Rheology. Dynamic storage and loss moduli, $G'(\omega)$ and $G''(\omega)$, of the various dendritic star polymers are shown in Figure 2, where several rheological features are apparent. First, at least two minima in $\tan(\delta)$ clearly appear for all samples, indicating there was a second plateau G_{II} due to the presence of more than one branch-point. Such a second plateau also has been observed in H-shaped,[2,8] multiarm,[6,8,11] and comb polymers[4,7−11] as a signature of the relaxation hierarchy. Moreover, three minima in $\tan(\delta)$ of 3GDSPBD G(5,6,32) and a slight hint of the third $\tan(\delta)$ minimum of 3GDSPBD G(5,6,5) in Figure 2c indicate there was another level of the relaxation hierarchy, which agrees with the expectation from the synthesis scheme. Therefore, linear viscoelastic responses, especially the number of minima in $\tan(\delta)$, can be used to identify the relaxation hierarchy (or the degree of generation) of given branched polymers. Second, arms with molecular weights a few times the entanglement molecular weight gave rise to a clear separation in relaxation dynamics showing the first and second $\tan(\delta)$ minima of 3GDSPBD in Figure 2c. The clearly observed second plateau region, characterized by the second $\tan(\delta)$ minimum, might be a result of the dilution effect on $G'(\omega)$ and $G''(\omega)$ by a dramatic decrease of the unrelaxed polymer fractions due to the dendritic topology. Third, when the outer arms were of the same or similar molecular weights, $G'(\omega)$ nearly overlapped at high frequency and $G''(\omega)$ continuously overlapped until the terminal relaxation was completed (see Figure 2a,c). This was contrary to the behavior for outer arms of different molecular weight as shown in Figure 2b.

In general, the relaxation behavior of these dendritic star polymers agreed with the expected consecutive arm relaxation process at each generation. However, Figure 2d provides an interesting comparison between second and third generations. The molecular weight of the outermost arms in 2GDSPBD G(14,12) and 3GDSPBD G(14,15,1) are almost identical. Moreover, the effect of the inner arm at the center of 3GDSPBD G(14,15,1) might be considered to be negligible when the dilution effect is considered ($\phi_{chem,G\text{-}1} = 0.0127$). Therefore, the relaxation dynamics of 3GDSPBD G(14,15,1) would be expected to be similar to those of 2GDSPBD G(14,12), because arm retraction at each generation is more sensitive to arm molecular weights as well as to the unrelaxed polymer fractions, rather than to the number of arms. Indeed, $G'(\omega)$ and $G''(\omega)$ for these molecules nearly overlapped at high frequencies regardless of the number of arms. However, the terminal relaxation of 3GDSPBD G(14,15,1) became much slower than that of 2GDSPBD G(14,12) even though the difference in arm molecular weights in the terminal region is less than two entanglement molecular weights.

This raises an interesting question about the degree of dilution in dendritic architectures. To estimate the degree of dilution by the faster relaxing outer arms, the rubbery plateau modulus G_N and the second plateau modulus G_{II} are evaluated as the average storage modulus values where each $\tan(\delta)$ minimum is observed. If the faster relaxing parts ideally act as an effective solvent immediately after their relaxation, the second plateau modulus should depend on the fraction of the unrelaxed parts ϕ_{eff} as $G_{II} = G_N \times \phi_{eff}^{\alpha+1}$ with the dilution exponent.[2−12] However, when the measured plateau ratios G_{II}/G_N are plotted against the unrelaxed polymer fractions $\phi_{chem,G\text{-}1}$ based on the evaluated arm molecular weights in Table 1, the degree of dilution deviates far from the expected dilution exponent $\alpha = 4/3$, as shown in Figure 2e. This finding would seem to violate the key assumption of dynamic dilution in arm retraction. It is plausible that a polymer chain with a highly branched architecture has more probability to entangle with its own segments than those of neighboring chains in the equilibrium melt state. This situation well satisfies the ideal self-dilution condition of the dynamic dilution assumption. However, current G_{II}/G_N analysis suggests the degree of dilution may decrease as branched architectures become more complicated. In the case of linear and three-arm star polymer solutions with oligomeric linear chains, the

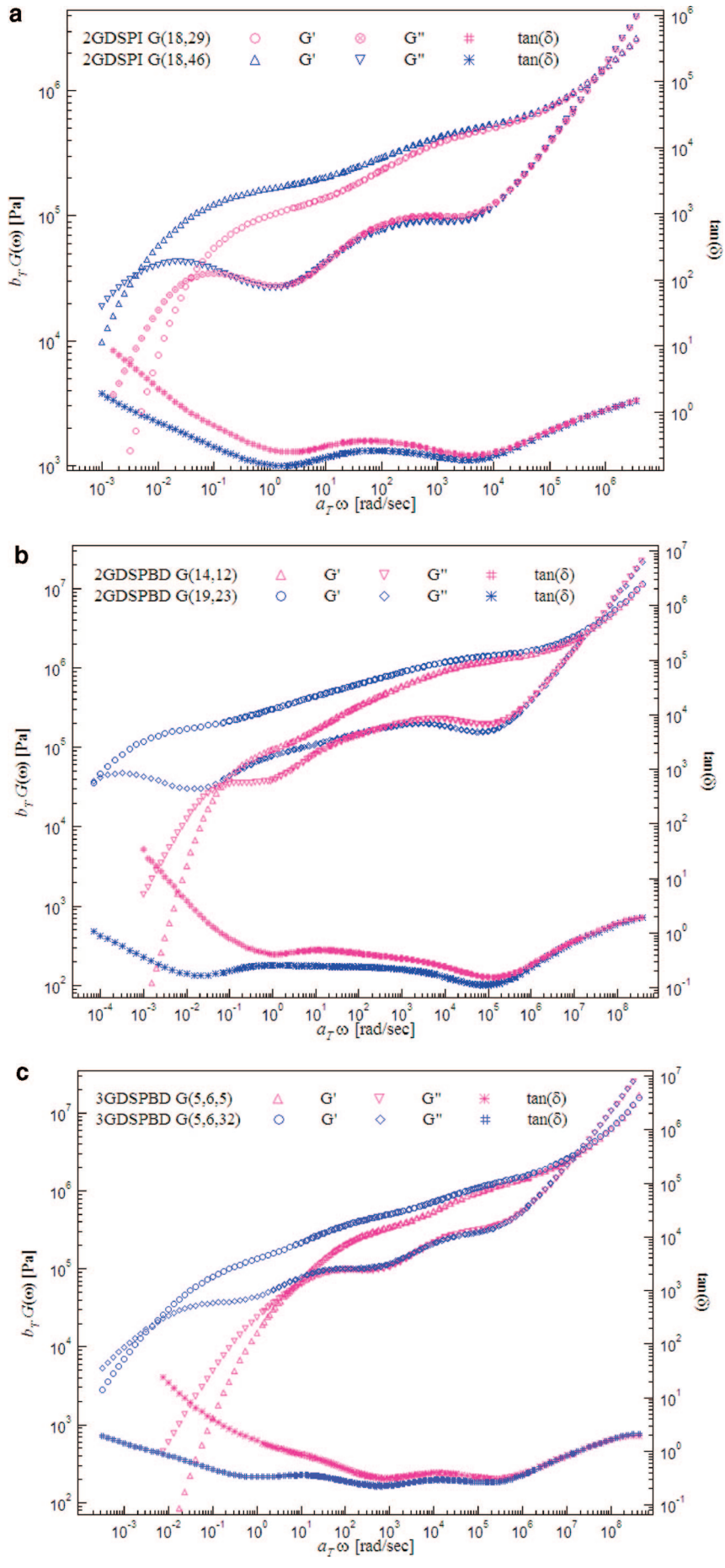
a
2GDSPI G(18,29) G' G'' tan(δ)
2GDSPI G(18,46) G' G'' tan(δ)
$b_T G(\omega)$ [Pa]
tan(δ)
$a_T\omega$ [rad/sec]
b
2GDSPBD G(14,12) G' G'' tan(δ)
2GDSPBD G(19,23) G' G'' tan(δ)
$b_T G(\omega)$ [Pa]
tan(δ)
$a_T\omega$ [rad/sec]
c
3GDSPBD G(5,6,5) G' G'' tan(δ)
3GDSPBD G(5,6,32) G' G'' tan(δ)
$b_T G(\omega)$ [Pa]
tan(δ)
$a_T\omega$ [rad/sec]

Figure 2.

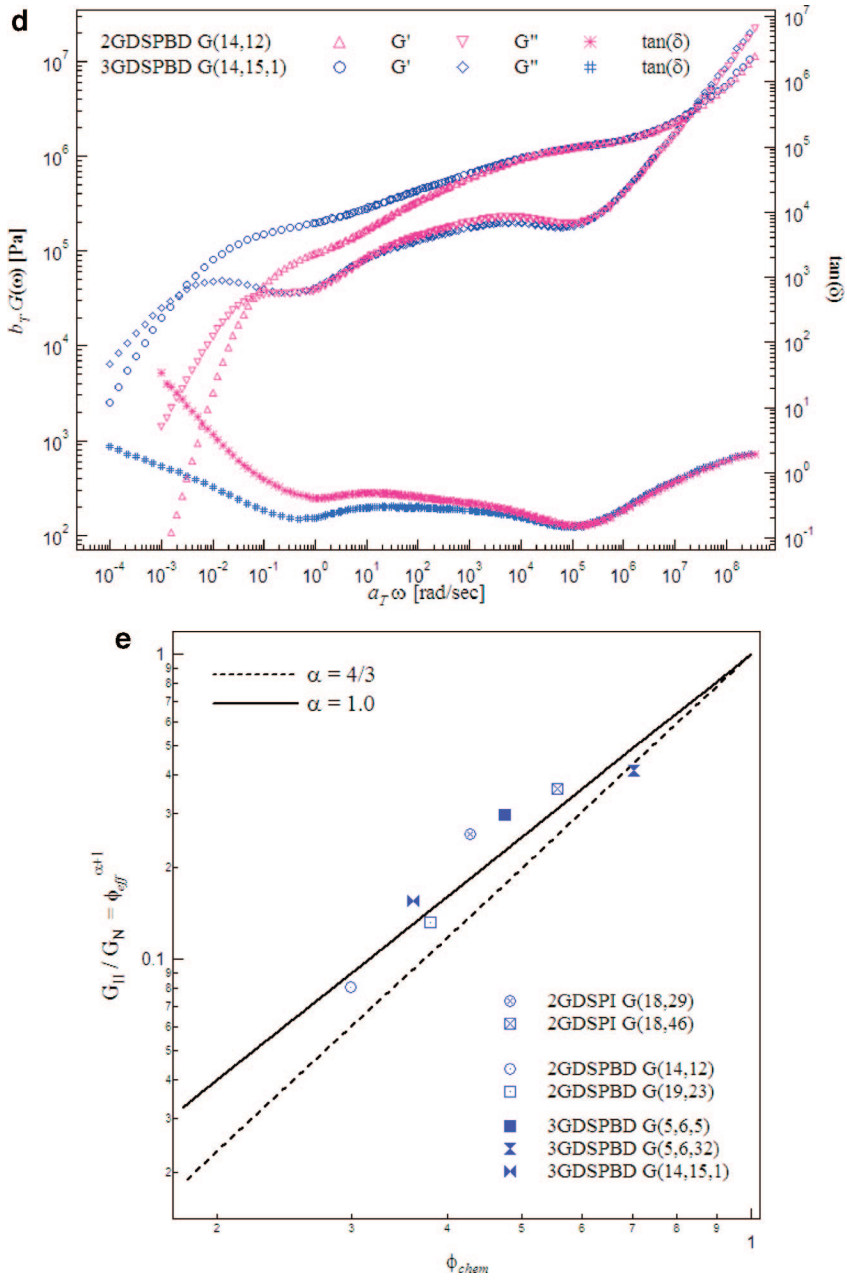

Figure 2. (a) Experimental storage and loss moduli as well as tan(δ) of 2GDSPI G(18,29) and 2GDSPI G(18,46) at T_{ref} = 28 °C. (b) Experimental storage and loss moduli as well as tan(δ) of 2GDSPBD G(14,12) an 2GDSPBD G(19,23) at T_{ref} = 28 °C. (c) Experimental storage and loss moduli as well as tan(δ) of 3GDSPBD G(5,6,5) and 3GDSPBD G(5,6,32) at T_{ref} = 28 °C. (d) Experimental storage and loss moduli as well as tan(δ) of 2GDSPBD G(14,12) and 3GDSPBD G(14,15,1) at T_{ref} = 28 °C. (e) Experimental plateau modulus ratios G_{II}/G_N for second and third generation dendritic star polymers, plotted against the unrelaxed polymer fractions based on the synthesis scheme ϕ_{chem}. Solid and dotted lines are the unrelaxed polymer fraction dependence of G_{II}/G_N with the dilution exponent α = 1 and 4/3, respectively.

experimentally evaluated α values from the measured G_{II}/G_N ratios were between 1.2 and 1.25.[20,21] On the other hand, α values between 1 and 4/3 were reported in comb or multiarm polymer melts and solutions.[7,9,11,12] Moreover, Watanabe et al. measured dielectric relaxation $\Phi(t)$ and stress relaxation $\mu(t)$ functions for binary linear/linear,[22] star/star,[23] and star/linear[24] polyisoprene polymer blends as well as second generation dendritic star polyisoprene[25] to examine the picture of dynamic tube dilation (dynamic dilution) caused by the faster relaxing chains. Their comparisons between $\Phi(t)$ and $\mu(t)$ suggested the relaxation of the faster relaxing parts itself might not always guarantee the expected fully dilated tube to the slower relaxing parts. That is, the relaxation of the slower relaxing parts in a fully dilated tube at given time occurs only when their entanglement unit segments in the original tube complete exploring the entire dilated tube before the given t. Thus, a time required for this exploring process determines the size of a recognized dilated tube (a partially dilated tube) with which the constraint-release mechanism governs the terminal dynamics of the unrelaxed parts. Therefore, it is possible the degree of dilution is not a simple constant. That is, α could be a collective parameter affected by multiple relaxation time scales, structural complexity, polydispersity at each generation or structural heterogeneity due to incomplete linking reactions.

Furthering order to explore the rheological features of dendritic architectures in more detail, the measured data were compared with the predictions of the hierarchy theory. As mentioned earlier, our main purpose is to find which parameters play the key roles in remedying any observed discrepancy between predictions and experiments, rather to add any new mechanism or modify the ones in the current model. The input parameters in the hierarchy theories are G_N, τ_e, M_e, p, q, and α.

Ideally, the values of G_N, M_e, and τ_e can be determined by experimental data with known polymer density ρ and monomer friction constant ζ_0, but the various theoretical studies[2−12] have used different values for α, p, and q. The value of α has varied among 1, 1.2, or 4/3 despite the theoretical expectation that it should be a simple constant with value 4/3. The value of q has varied depending on the given architecture, either the number of arms per branch-point in H-shaped and multiarm polymers or the number of branch-points in comb polymers.[2−12] Also, the normalized hopping barrier p has been chosen as a constant, either 1 or 1/12, regardless of the given architectures[2,4−12] or suggested as a function of the given architectures[8] (the entanglement density of unrelaxed parts). Therefore, it will be interesting to examine which parameter dominantly governs the accuracy of the predictions from the hierarchy model.

The average of measured G_N and the resulting $M_e = \rho RT/G_e = (4/5)\rho RT/G_{N,avg}$ of dendritic polybutadienes ($\rho = 0.895$ g/cm^3) are $G_{N,avg} = 1.235$ ($\pm$ 0.102) MPa and $M_e = 1.451$ kg/mol, and those of dendritic polyisoprenes ($\rho = 0.9$ g/cm^3) are $G_{N,avg} = 0.461$ ($\pm$ 0.021) MPa and $M_e = 3.908$ kg/mol. However, the values of G_N and τ_e in current approach are fixed as $G_{Nf} = 0.6$ MPa and $\tau_{ef} = 7.4$ μs for polyisoprenes, and $G_{Nf} = 1.42$ MPa and $\tau_{ef} = 0.22$ μs for polybutadienes to match the crossover between $G'(\omega)$ and $G''(\omega)$ at the high frequency region and the rubbery plateau region as used in the earlier studies.[2,4,8,10] The value of q is fixed as the number of branch-points per inner arm and p^2 is the inverse of the entanglement density of the unrelaxed inner parts.

Due to the symmetric nature of a dendritic architecture, the relaxation dynamics are governed by the inner arm (M_{G-1}) retraction following the outer arm (M_{G-2}) retraction of a Y-shaped section in 2GDS. The outer arm (M_{G-2}) relaxation mechanism is the same as the arm retraction with the unrelaxed inner arm fraction as expressed in asymmetric star or comb polymers.[1−10] The early fluctuation time of M_{G-2} is computed from the curvilinear Rouse motion (equivalent to the contour length fluctuation CLF),[4,7,8,10] such that $\tau_{early,G-2}(s_{G-2}) = (9\pi^3/16)\tau_e(N_{G-2}/N_e)^4(s_{G-2})^4$ with a fractional distance from the free end s_{G-2} and the number of monomer in an entanglement strand $N_e = M_e/m_0 = a_0^2/b^2$. Here m_0 is the monomer molecular weight, a_0 is the original tube diameter, and b is the (Kuhn) monomer length. The arm relaxation time of M_{G-2} is determined with the effective potential $U_{eff,G-2}$ as follows

$$Z_{G-2} = N_{G-2}/N_e \tag{1}$$

$$U_{eff,G-2}(s_{G-2}) = 3Z_{G-2}\frac{1-(1-\phi_{G-2}s_{G-2})^{\alpha+1}[1+(1+\alpha)\phi_{G-2}s_{G-2}]}{\phi_{G-2}^2(\alpha+1)(\alpha+2)} \tag{2}$$

$$\tau_{late,G-2}(s_{G-2}) = \sqrt{\frac{\pi^5}{6}}\tau_e Z_{G-2}^{3/2} \times \frac{\exp[U_{eff,G-2}(s_{G-2})]}{\sqrt{s_{G-2}^2(1-\phi_{G-2}s_{G-2})^{2\alpha} + \frac{1}{\phi_{G-2}^2}\left(\frac{\phi_{G-2}^2(1+\alpha)}{3Z_{G-2}}\right)^{2\alpha/(1+\alpha)}\left(\Gamma\left[\frac{1}{1+\alpha}\right]\right)^{-2}}} \tag{3}$$

$$\tau_{G-2}(s_{G-2}) = \frac{\tau_{early,G-2}(s_{G-2})\exp[U_{eff,G-2}(s_{G-2})]}{1+\tau_{early,G-2}(s_{G-2})\exp[U_{eff,G-2}(s_{G-2})]/\tau_{late,G-2}(s_{G-2})} \tag{4}$$

After the outer arm relaxation, the mobility of the branch-point $D_{eff,G-1} = kT/\zeta_{total}$ can be expressed in terms of total drag friction $\zeta_{total} = \zeta_{C,G-1} + q\zeta_{bp}$ due to the inner arm monomeric friction $\zeta_{C,G-1} = (N_{G-1}\zeta_0)$ and the drag friction at the branch-point by already relaxed outer arms $\zeta_{bp} = kT[2\tau_{G-2}(1)/(pa_0)^2]$.[5,8] Here $N_{G-1} = M_{G-1}/m_0$ is the number of monomers in the inner arm, ζ_0 is the monomer friction coefficient, $p^2 = a_0^2/(N_{G-1}b^2) = N_e/N_{G-1}$ is self-consistently determined from the unrelaxed inner arm (e.g., M_{G-1}), and q is the number of branch-points in the Y-shaped section. The early fluctuation time of M_{G-1}, by analogy to a free Rouse chain,[4,7,8,10] is given by $\tau_{early,G-1}(s_{G-1}) = (L_{G-1}s_{G-1})^2/(2D_{eff,G-1}) + \tau_{G-2}(1)$ where the second term[3] $\tau_{G-2}(1)$ is to maintain the continuity of relaxation time scale at the branch-point. Writing the effective contour length of the inner arm as $L_{G-1} = N_{G-1}b^2\phi_{G-1}^{\alpha/2}/a_0$, the arm relaxation time of M_{G-1} is determined with the effective potential $U_{eff,G-1}$ as follows

$$Z_{G-1} = N_{G-1}/N_e \tag{5}$$

$$U_{eff,G-1}(s_{G-1}) = 3Z_{G-1}\phi_{G-1}^{\alpha}\frac{1-(1-s_{G-1})^{\alpha+1}[1+(1+\alpha)s_{G-1}]}{(\alpha+1)(\alpha+2)} \tag{6}$$

$$\tau_{late,G-1}(s_{G-1}) = \frac{L_{G-1}^2}{D_{eff,G-1}}\sqrt{\frac{2\pi}{3Z_{G-1}\phi_{G-1}^{\alpha}}} \times \frac{\exp[U_{eff,G-1}(s_{G-1})]}{3Z_{G-1}\phi_{G-1}^{\alpha}\sqrt{s_{G-1}^2(1-s_{G-1})^{2\alpha} + \left(\frac{1+\alpha}{3Z_{G-1}\phi_{G-1}^{\alpha}}\right)^{2\alpha/(1+\alpha)}\left(\Gamma\left[\frac{1}{1+\alpha}\right]\right)^{-2}}} \tag{7}$$

The first approach was to check the validity of the measured plateau ratio G_{II}/G_N. The measured $G_{II}/G_N = \phi_{eff}^{\alpha+1}$ only depends on the relaxed and unrelaxed fractions regardless of the choice of G_N, τ_e, M_e, p, and q. If $\alpha = 4/3$ is assumed, ϕ_{eff} will give an adjusted M_{G-1}* in 2GDS because ϕ_{eff} is $3M_{G-1}$*/$(3M_{G-1}* + 6M_{G-2})$, and M_{G-2} is more accurately quantified than M_{G-1}, which is calculated from the molecular weight of the intermediate star dendron. Therefore, all parameters except M_{G-1}* were fixed as G_{Nf}, τ_{ef}, M_e, $q = 1$, and $\alpha = 4/3$. Specifically, p^2 was self-consistently determined as N_e/N_{G-1}* by M_{G-1}*. Figure 3a,b shows a good agreement between the measured data and the predictions with M_{G-1}*. As expected from the smaller α values in Figure 2e, all values of M_{G-1}* became larger than measured M_{G-1}. For example, M_{G-1}* of 2GDSPBD G(19,23) was 27.3823 kg/mol, indicating $M_{G-1}* = M_{G-1} + M_\alpha$. It is possible M_{G-1} obtained by SEC-TALLS was less accurately evaluated than a real molecular weight because the conventional SEC method was not able to isolate M_{G-1} only from the intermediate star dendron (e.g., $2M_{G-2} + M_{G-1}$). However, the problem of this approach (fixed α and adjusted M_{G-1}*) is the choice of α changes the value of M_{G-1}*. If $\alpha = 1$ is chosen, another set of M_{G-1}* would be obtained. Therefore, the question of whether the degree of dilution α is a universal constant for all different branched architectures remains to be resolved and so far the results on this score are inconclusive.

The second approach was to examine how effectively p and q parameters affected the model predictions. In this approach, p and q were treated as fitting parameters to match the terminal $G'(\omega)$ and $G''(\omega)$ crossover, while G_{Nf}, τ_{ef}, M_{G-1}, M_{G-1}, and $\alpha = 4/3$ were fixed. Figure 3c shows the predictions with different p, q, and M_e of 2GDSPBD G(19,23). In the case of using the measured $M_e = 1.451$ kg/mol, the predictions required p^2 to be 1/40, which is significantly smaller than 1/12 or 1, to reach the terminal $G'(\omega)$ and $G''(\omega)$ crossover. This p^2 value implies the branch-point only moves about 1/6 of the original tube distance at each cycle of the outer arm relaxation. Also, increasing q from 1 to 2 made the inner relaxation slower at the terminal region but the magnitude of $G'(\omega)$ and $G''(\omega)$ was still underestimated. Thus, none of these parameters corrected the observed discrepancies, especially $G'(\omega)$ and $G''(\omega)$ at the terminal region. If $M_{e*} = 1.8$ kg/mol was chosen as used in earlier theoretical studies of star and comb polybutadienes,[1,4,10] the predictions with $q = 2$ and $p^2 = 1/200$ produced more

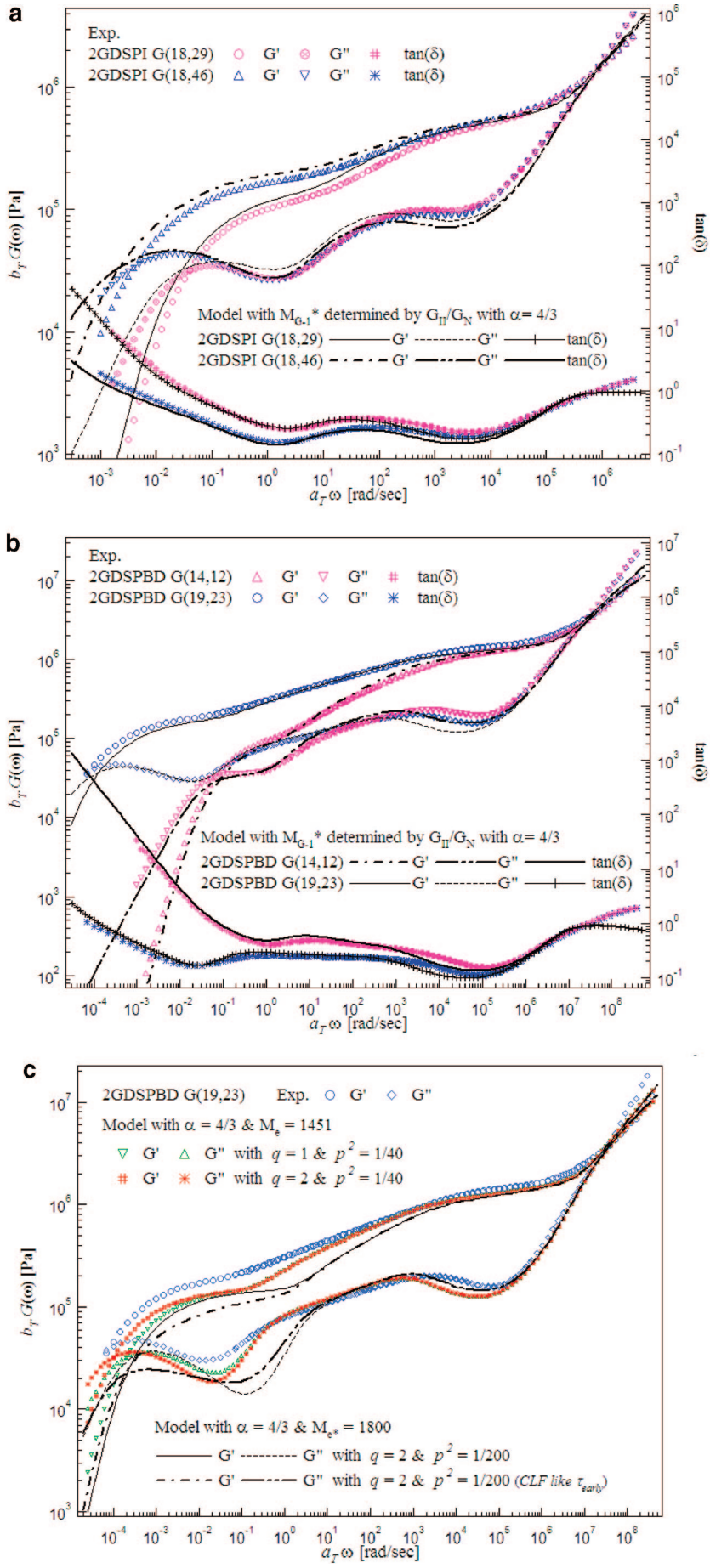
a
Exp.
2GDSPI G(18,29) G' G'' tan(δ)
2GDSPI G(18,46) G' G'' tan(δ)
Model with M_G-1* determined by G_II/G_N with α= 4/3
2GDSPI G(18,29) G' G'' tan(δ)
2GDSPI G(18,46) G' G'' tan(δ)
b_T·G(ω) [Pa]
tan(δ)
a_T·ω [rad/sec]
b
Exp.
2GDSPBD G(14,12) G' G'' tan(δ)
2GDSPBD G(19,23) G' G'' tan(δ)
Model with M_G-1* determined by G_II/G_N with α= 4/3
2GDSPBD G(14,12) G' G'' tan(δ)
2GDSPBD G(19,23) G' G'' tan(δ)
b_T·G(ω) [Pa]
tan(δ)
a_T·ω [rad/sec]
c
2GDSPBD G(19,23) Exp. G' G''
Model with α = 4/3 & M_e = 1451
G' G'' with q = 1 & p^2 = 1/40
G' G'' with q = 2 & p^2 = 1/40
Model with α = 4/3 & M_e* = 1800
G' G'' with q = 2 & p^2 = 1/200
G' G'' with q = 2 & p^2 = 1/200 (CLF like τ_early)
b_T·G(ω) [Pa]
a_T·ω [rad/sec]

Figure 3.

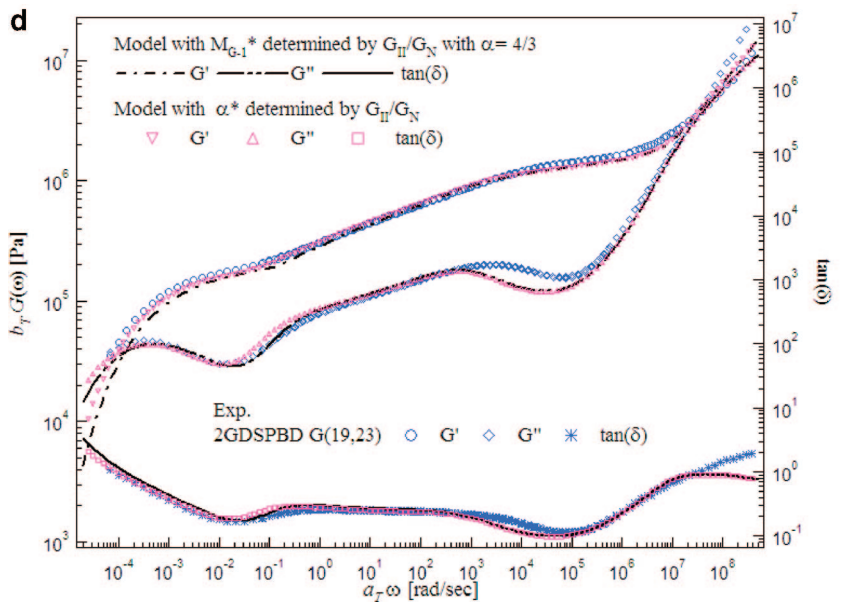

Figure 3. (a) Comparison of experimental and theoretical viscoelastic properties of 2GDSPI G(18,19) and 2GDPI G(18,46). The symbols are the measured data and the lines are the model predictions with the adjusted inner arm molecular weight $M^*_{G\text{-}1}$. (b) Comparison of experimental and theoretical viscoelastic properties of 2GDSPBD G(14,12) and 2GDPBD G(19,23). The symbols are the measured data and the lines are the model predictions with the adjusted inner arm molecular weight $M^*_{G\text{-}1}$. (c) Comparison of experimental and theoretical viscoelastic properties of 2GDSPBD G(19,23). The measured data are circle and diamond symbols. The other symbols and lines are the model predictions with the adjusted p and q parameters (see text). (d) Comparison of experimental and theoretical viscoelastic properties of 2GDSPBD G (19,23): the measured data (○, ◇, ∗), the model predictions with the adjusted inner arm molecular weight $M^*_{G\text{-}1}$ (−•−, −••−, —), the model predictions with the adjusted dilution exponent α* (▽, △, □).

deviations, even at the intermediate frequencies, as shown in Figure 3c. The inner arm relaxation with $\tau_{early,G\text{-}1}$ based on either the free Rouse motion or the curvilinear Rouse motion underestimated the magnitude more with $M_{e*} = 1.8$ kg/mol. This comparison suggests the adjusting p and q is not as effective to remedy the discrepancies as are the adjusting arm molecular weights (or the resulting unrelaxed fraction) and the choice of M_e, which emphasizes the importance of the entanglement density at each generation.

The last approach we tried was to use α* as an adjustable parameter. We used the measured $G_{II}/G_N = \phi_{eff}^{\alpha+1}$ with $\phi_{eff} = \phi_{chem,G\text{-}1}$ to provide an adjusted α* value for each 2GDS. Under the assumption that the desired architecture had been achieved in the synthesis, any deviation from $\phi_{chem,G\text{-}1}$, which comes from any imperfect linking reaction or unknown effect of a given topology, will appear in the measured G_{II} with α*. In this approach, the input parameters are G_{Nf}, τ_{ef}, M_e, $M_{G\text{-}1}$, $M_{G\text{-}2}$, $q = 1$, $p^2 = N_e/N_{G\text{-}1}$ were fixed, while α* was determined from the measured G_{II}/G_N as $[\log(G_{II}/G_N)/\log(\phi_{chem,G\text{-}1})] - 1$. Figure 3d shows a good agreement with not only the experiments but also the predictions with $M_{G\text{-}1}$*. A more unexpected finding with α* was the accuracy of the predictions of the outer arm dynamics but not that of the terminal inner arm relaxation. That is, the effect of a faster dilution of $\alpha = 4/3$ with a larger $M_{G\text{-}1}$* on the terminal dynamics could be compensated with the effect of a slower dilution of α* with a smaller $M_{G\text{-}1}$. However, the predicted $G'(\omega)$ and $G''(\omega)$ at the intermediate frequencies, governed by the outer arm relaxation, nearly overlapped each other, even for two different α and ϕ values are used as shown in Figure 3d. One possible explanation could be a weaker ϕ and α dependence of the outer arm modulus contribution, $(\alpha + 1) \times \phi_{chem,G\text{-}2}$, compared with that of the inner arm modulus contribution $(\alpha + 1) \times (\phi_{chem,G\text{-}1})^{\alpha+1}$.[2−10] To examine whether α* can predict the measured data consistently, this approach was applied to all the 2GDS and 3GDS polymers.

The theoretical descriptions of relaxation dynamics for 3GDS were similar to those for 2GDS with the additional relaxation modes of the middle arm ($M_{G\text{-}2}$ in 3GDS) with the unrelaxed fraction ($\phi_{eff,G\text{-}2} = \phi_{chem,G\text{-}1} + \phi_{chem,G\text{-}2}$). The effective potential $U_{eff,G\text{-}2}$, which is similar to the earlier formulation used for the end effect in comb polymers,[4,7,9,10] and the relaxation times are as follows with $L_{G\text{-}2} = N_{G\text{-}2}b^2\phi_{eff,G\text{-}2}^{\alpha/2}/a_0$ and $D_{eff,G\text{-}2} = kT/[N_{G\text{-}2}\zeta_0 + q2\tau_{G\text{-}3}(1)/(pa_0)^2]$

$$g = \frac{\phi_{G\text{-}2}}{\phi_{G\text{-}2} + \phi_{G\text{-}1}} = \frac{\phi_{G\text{-}2}}{\phi_{eff,G\text{-}2}} \tag{8}$$

$$U_{eff,G\text{-}2}(s_{G\text{-}2}) = 3Z_{G\text{-}2}\phi_{eff,G\text{-}2}^{\alpha}\frac{1-(1-gs_{G\text{-}2})^{\alpha+1}[1+(1+\alpha)gs_{G\text{-}2}]}{g^2(\alpha+1)(\alpha+2)} \tag{9}$$

$$\tau_{early,G\text{-}2}(s_{G\text{-}2}) = (L_{G\text{-}2}s_{G\text{-}2})^2/(2D_{eff,G\text{-}2}) + \tau_{G\text{-}3}(1) \tag{10}$$

$$\tau_{late,G\text{-}2}(s_{G\text{-}2}) = \frac{L_{G\text{-}2}^2}{D_{eff,G\text{-}2}}\sqrt{\frac{2\pi}{3Z_{G\text{-}2}\phi_{eff,G\text{-}2}^{\alpha}}} \times \frac{\exp[U_{eff,G\text{-}2}(s_{G\text{-}2})]}{3Z_{G\text{-}2}\phi_{eff,G\text{-}2}^{\alpha}\sqrt{s_{G\text{-}2}^2(1-gs_{G\text{-}2})^{2\alpha} + \frac{1}{g^2}\left(\frac{g^2(1+\alpha)}{3Z_{G\text{-}2}\phi_{eff,G\text{-}2}^{\alpha}}\right)^{2\alpha/(1+\alpha)}\left(\Gamma\left[\frac{1}{1+\alpha}\right]\right)^{-2}}} \tag{11}$$

Using α* led to reasonable predictions for all 2GDS as shown in Figure 4a,b, while the same approach yielded poor predictions for 3GDS, especially in the terminal region (see Figure 4c). The relaxation dynamics of the outer and the middle arms, for example, of 3GDSPBD G(5,6,32), were well predicted. However, the predicted terminal dynamics seriously deviated from the experiments showing opposite trends, a faster terminal relaxation of 3GDSPBD (5,6,5) and a slower terminal relaxation of 3GDSPBD (5,6,32). It is possible there are missing relaxation mechanisms in higher generation dendritic architectures. Also it should be noted that the calculated molecular weight of the innermost arm ($M_{w,G\text{-}1}$) of 3GDS probably contained more error

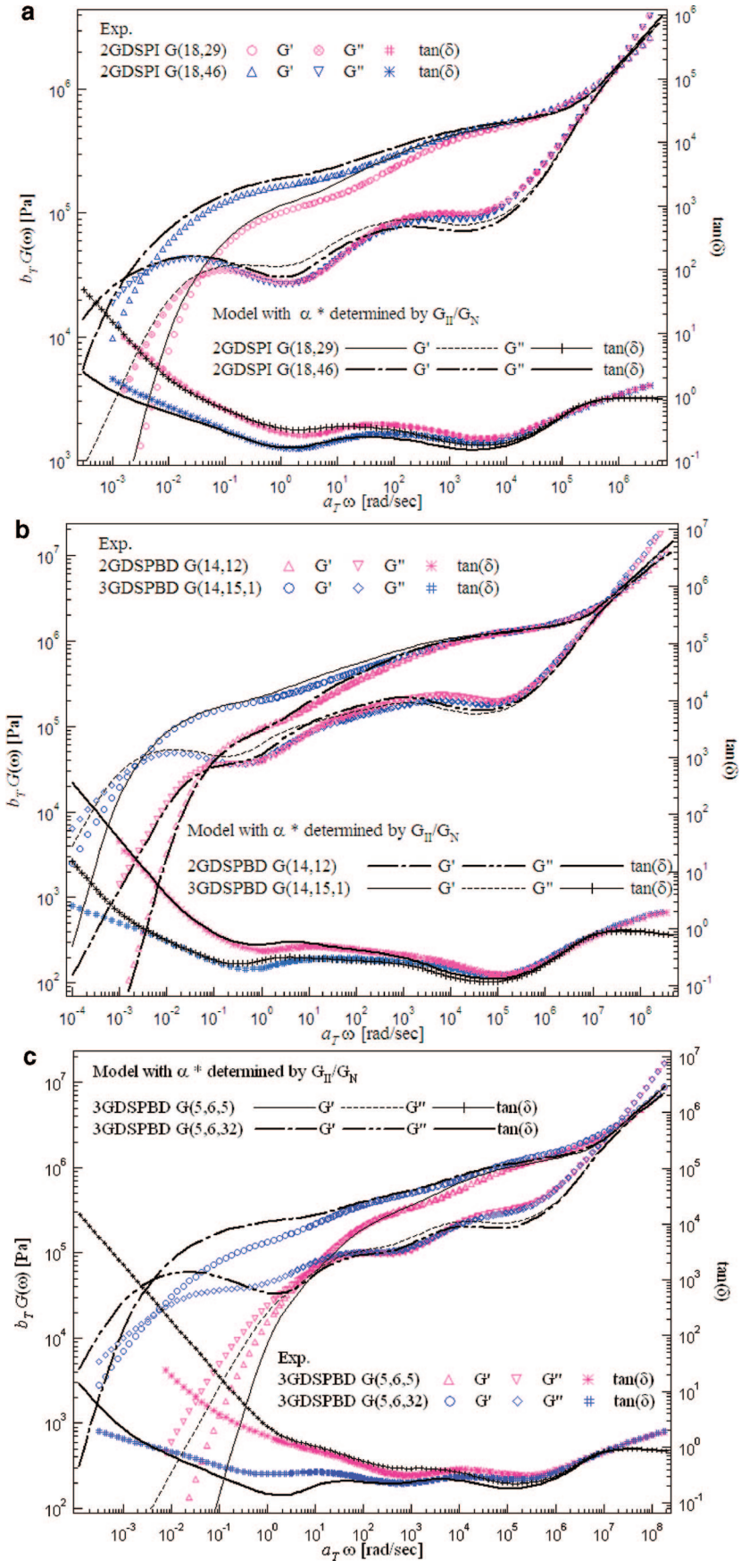

Figure 4. (a) Comparison of experimental and theoretical viscoelastic properties of 2GDSPI G(18,29) and 2GDPI G(18,46). The symbols are the measured data and the lines are the model predictions with the adjusted dilution exponent α*. (b) Comparison of experimental and theoretical viscoelastic properties of 2GDSPBD G(14,12) and 3GDPBD G(14,15,1). The symbols are the measured data and the lines are the model predictions with the adjusted dilution exponent α*. (c) Comparison of experimental and theoretical viscoelastic properties of 3GDSPBD G(5,6,5) and 3GDPBD G(5,6,32). The symbols are the measured data and the lines are the model predictions with the adjusted dilution exponent α*.

because typical SEC-TALLS method could not characterize $M_{w,G\text{-}1}$ alone from the intermediate star dendron units building the third generation architectures. Then, small changes in arm molecular weights in 3GDS will dramatically alter the unrelaxed fractions and further relaxations. However, it is apparent that the predictions with α^* yields a better agreement than those with either $\alpha = 4/3$ or 1 under the same model framework. This method could lead to an alternative way to understand that data, by regarding α as a collective parameter, determined from the measured G_{II}/G_N, and reflecting possible nonidealities in the complex architectures, rather to add new relaxation modes in order to predict the measured data.

Fitting the measured linear viscoelastic data with above three model approaches suggest that (1) p and q parameters represent key physics in the relaxation mechanisms of branched polymers, but adjusting p and q may not so effectively improve the accuracy of predictions as does adjusting effective arm molecular weight or the dilution exponent; and (2) adjusting $M_{G\text{-}1}^*$ or α^* implies the relaxation dynamics of dendritic architectures are affected by topological effects causing a slower relaxation than the predictions of current hierarchy theory. Intuitively, incomplete linking reactions are expected in current complex dendritic topology and the resulting structural heterogeneity will lead to faster relaxation dynamics in experimental data than theoretical predictions assuming the perfect dendritic topology. In spite of this expectation, the hierarchical theory predicted faster relaxation dynamics if arm molecular weights or the values of α were not adjusted. One possible source of the predicted faster dynamics is the inaccuracy of characterized arm molecular weights at each generation. However, adjusting inner arm molecular weight to fit the measured data yields the total molecular weight with $M_{G\text{-}1}^*$ larger than the total molecular weight of the final product, which is either measured by SEC-TALL or calculated as the sum of all arms in Table 1 (for example, around 50 kg/mol differences in 2GDSPI series). The other source is to invoke some missing relaxation mode for dendritic architectures as suggested by van Ruymbeke et al.,[12] but the added new concept with renormalized arm lengths still needs $\alpha = 1$ instead of $\alpha = 4/3$. It is difficult to pinpoint the effect of dendritic topology on the relaxation dynamics without accurate molecular characterizations for arm molecular weights, polydispersity at each generation and structural heterogeneity due to possible imperfect linking reactions in the complicated multiple-step synthesis, while the observed trend, increased $M_{G\text{-}1}^*$ and smaller α^*, could be a sign of a relatively slower rate of dilution effect than the theoretical expectation due to the complex topology with multiple arms and generations implying some missing physics in the seemingly successful hierarchy theories claiming no adjustable parameter. A simple attempt to incorporate the dilution effect by adjusting model parameters such as α shows the limit of the current model framework as the number of branching generations increases, which shows the need to develop new theories to reflect the tube dilution with time (e.g., a time-dependent dilution exponent) at the expense of the simplicity of the current hierarchy theories. Details of such topological effects are not yet understood so further studies with advanced analytical methods such as temperature gradient interaction chromatography[26,27] (TGIC), which can eliminate some of uncertainties in molecular characterizations, are still needed.

3.2. Nonlinear Relaxation Modulus after Step Strains. The relaxation moduli, $G(t,\gamma)$, of 2GDSPBD G(14,12), 2GDSPI G(18,29) and 3GDSPBD G(5,6,5) measured after the imposition of step strains are provided in Figure 5. At low strains these overlap at all times, but at some value of strain $G(t,\gamma)$ began to decrease as strain increased. The former behavior is a characteristic of the linear deformation regime, while the latter strain dependence of $G(t,\gamma)$ indicates that the polymer was in the nonlinear deformation regime.[14,15] In general, shifting $G(t,\gamma)$ along the y-axis by an amount of $h(\gamma)$ yields almost overlapping $G(t,\gamma)h(\gamma)^{-1}$ at long times regardless of applied strains, indicating the time-strain factorability,[14,15] as shown in Figure 5b. The characteristic separability time of 2GDSPBD G(14,12) was around 30 s. The nonlinear relaxation moduli $G(t,\gamma)$ of 2GDSPI G(18,29) and 3GDSPBD G(5,6,5) at long times (beyond the evaluated longest relaxation times of $\tau_{\eta''} = 50$ s and $\tau_{\eta''} = 1.8$ s, respectively) were nearly parallel, as shown in Figure 5c,d, even though the expected time-strain factorability with a characteristic separability time was not seen. That is, overlap of $G(t,\gamma)h(\gamma)^{-1}$ for 2GDSPI G(18,29) could be obtained with a certain separability time (around 45 s in Figure 5e), but at some longer times $G(t,\gamma)h(\gamma)^{-1}$ at various strains no longer overlapped. A careful inspection of Figure 5e reveals that the behavior of $G(t,\gamma)h(\gamma)^{-1}$ separated into two groups. All of the measurements for $\gamma < 2.0$ overlapped at long times with the rest of those in that group, and similarly, all measurements for $\gamma > 2.0$ overlapped with each other, but the two groups did not overlap. In the case of 3GDSPBD G(5,6,5), the time-strain separability seemed to be only approximate, as shown in Figure 5f. These results also imply that the separability time was uncertain. It is true that the torque signal became unreliable at long times as it approached its lower limit. On the other hand, the obtained poor time-strain separability could be a result of experimental artifacts such as interfacial wall-slip or strain inhomogeneities.[15] Such experimental instabilities are believed to cause type C damping behavior, which well-entangled linear polymer melts/solutions usually produce, although the physical origins of type C are not well understood. If any experimental artifact indeed occurred, the corresponding damping behavior should have clearly exhibited kinklike type C behavior by being below the universal damping h_{DE} even at $\gamma < 1.0$.

In topological analogy with 2GDSPBD G(14,12), the strain-dependent damping function was quantified as $h(\gamma) = G(\gamma,t)/G(t)$. Figure 6a provides the corresponding damping function $h(\gamma,t)$ of 2GDSPBD G(14,12) at various discrete times. Here, h_{DE} and $h_{DE\text{-}IA}$ are the predictions of the Doi−Edwards damping theory without and with the independent alignment assumption. At short times, the measured damping function of 2GDSPBD G(14,12) exhibited less strain softening than h_{DE} and $h_{DE\text{-}IA}$ at low strains, but became parallel to the Doi−Edwards predictions at $\gamma \geq 4.0$. As time gradually increased, the measured damping function, especially at low strains, approached the Doi−Edwards predictions. At long times (beyond the evaluated longest relaxation time $\tau_{\eta''} = 25$ s), $h(\gamma,t)$ of 2GDSPBD G(14,12) at all strains became comparable to the Doi−Edwards damping function. It is obvious that the damping function of 2GDSPBD G(14,12) exhibits a transition from less strain softening (type B) to the universal Doi−Edwards damping (type A) at short times. The observed damping behavior, including the transition at short times, is consistent with the measured $h(\gamma,t)$ of multiarm polybutadiene polymers by Archer and Juliani.[19] In the case of 2GDSPI G(18,29), the corresponding $h(\gamma,t)$ in Figure 6b exhibits a similar transition in damping behavior despite the poor time-strain separability. Again, the effect of inner arm stretching appeared as less strain softening behavior at short times and exhibited the damping transition to h_{DE}, for example, at $t = 5$ s and at $\gamma \geq 6$. At long times, the $h(\gamma,t)$ of 2GDSPI G(18,29) for all strains followed the Doi−Edwards damping. Therefore, the observed damping transition is a rheological characteristic of not only H-shaped or multiarm architectures[2,18,19] but also the second generation dendritic architecture.

The presence of branch-point withdrawal for polymers with a dendritic topology is not surprising because 2GDS molecules consists of three symmetric Y-shape units where the branch-point

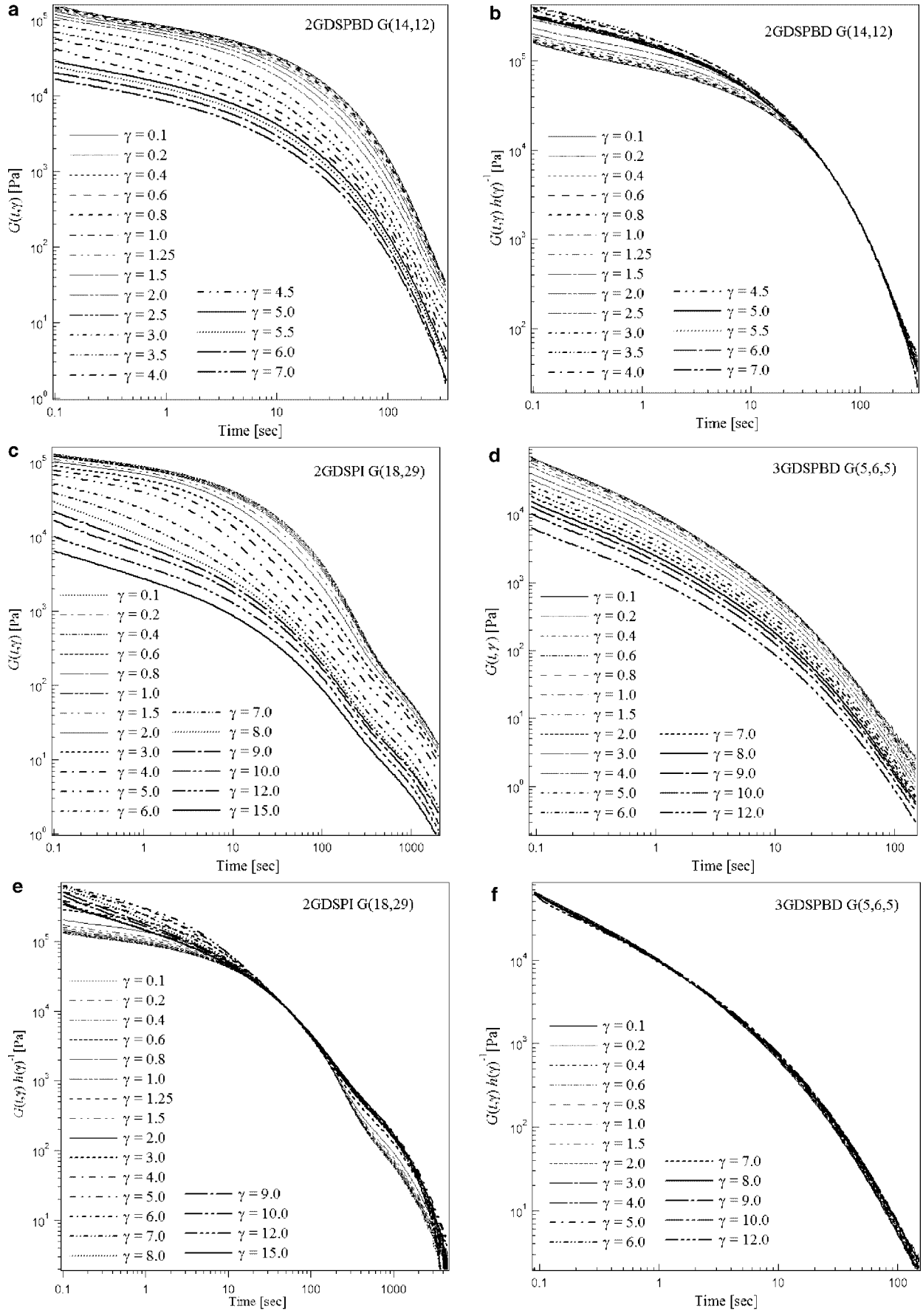

Figure 5. (a) Nonlinear shear relaxation moduli $G(t,\gamma)$ of 2GDSPBD G(14,12) after the imposition of step strains γ. (b) Shifted nonlinear shear relaxation moduli $G(t,\gamma)h(\gamma)^{-1}$ of 2GDSPBD G(14,12). (c) Nonlinear shear relaxation moduli $G(t,\gamma)$ of 2GDSPI G(18,29) after the imposition of step strains γ. (d) Nonlinear shear relaxation moduli $G(t,\gamma)$ of 3GDSPBD G(5,6,5) after the imposition of step strains γ. (e) Shifted nonlinear shear relaxation moduli $G(t,\gamma)h(\gamma)^{-1}$ of 2GDSPI G(18,29). (f) Shifted nonlinear shear relaxation moduli $G(t,\gamma)h(\gamma)^{-1}$ of 3GDSPBD G(5,6,5).

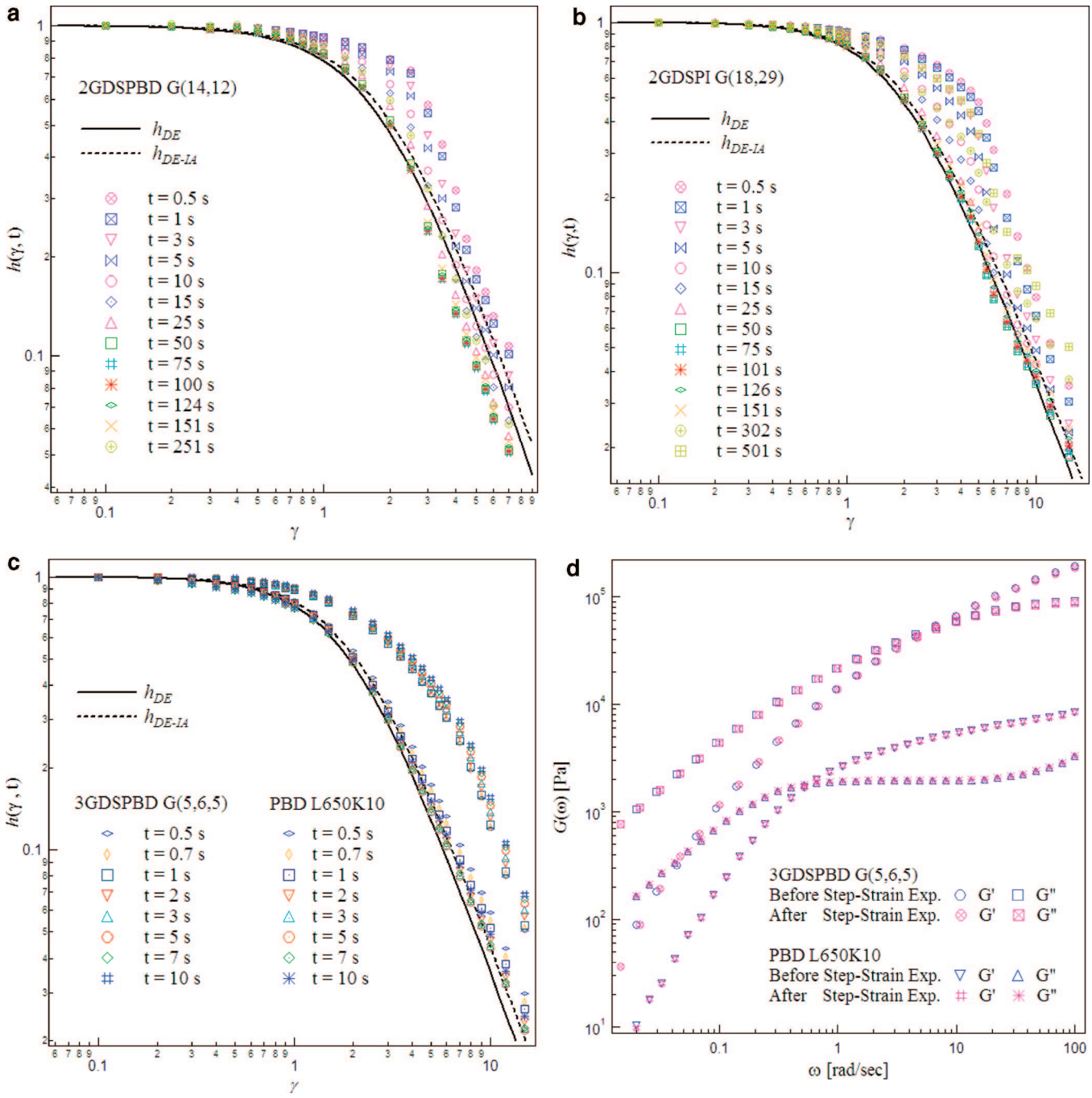

Figure 6. (a) Step shear damping function $h(\gamma,t)$ of 2GDSPBD G(14,12) at various times after the imposition of step strains. Lines are the predictions of the Doi−Edwards damping theory without and with the independent alignment assumption. (b) Step shear damping function $h(\gamma,t)$ of 2GDSPI G(18,29) at various times after the imposition of step strains. Lines are the predictions of the Doi−Edwards damping theory without and with the independent alignment assumption. (c) Step shear damping function $h(\gamma,t)$ of 3GDSPBD G(5,6,5) and PBD L650K10 at various times after the imposition of step strains. Lines are the predictions of the Doi−Edwards damping theory without and with the independent alignment assumption. (d) Dynamic moduli $G'(\omega)$ and $G''(\omega)$ of 3GDSPBD G(5,6,5) and PBD L650K10 before and after the step-strain experiments.

pulling motion occurs like that for the H-shaped or multiarm architectures. Theoretically, the branch-point withdrawal motion is expected when the inward tension generated by the stretched inner part $F_T = (3kT/a_D) <\boldsymbol{E}\cdot\boldsymbol{u}>$ overcomes the outward thermal force exerted by the free end $f_{th} = 3kT/a_0$, which comes from the arbitrary motion of the free end just outside of the confining tube.[2,16,17] A simple force balance of the Y-section with an approximation $<\boldsymbol{E}\cdot\boldsymbol{u}> \approx [1 + (4/15)\gamma^2)]^{0.5}$ suggests the branch-point withdrawal motion of 2GDSPI G(18,29) occurred at either $\gamma > 6.5$ for $a_D = a_0/(\phi_{chem})^{\alpha/2}$ or $\gamma > 3.4$ for $a_D = a_0$.[19] These theoretical strains are near (or less than) the strains where the damping transition was observed experimentally. However, it is difficult to quantify an exact theoretical strain with current experimental data because the measured damping transitions are also affected by the observation time. Considering that the tension balance is affected by the size of the confining tube, which, at a given time, is determined by the exploring process of the entanglement unit segments (discussed in section 3.1 as "a partially dilated tube"), the onset of the withdrawal motion is expected to change with time. The effect of observation time on $h(\gamma,t)$ is complicatedly related to the size of the dilated tube, the stretching relaxation dynamics of the inner parts of the entire molecules and the orientation of the outer parts induced by the withdrawal motion. These theoretical details are obviously important, but not the focus of current experimental study exploring rheological characteristics of dendritic topology. It

is also noteworthy that any hint of type C behavior did not appear in the corresponding $h(\gamma,t)$ of 2GDSPI G(18,29), which implies that the poor time-strain factorability may not be the result of experimental artifacts. On the other hand, there was unusual $h(\gamma,t)$ behavior at very long times which might be related to the poor time-strain factorability. At very long times, the $h(\gamma,t)$ shifted back to the $h(\gamma,t)$ at short times, as shown in Figure 6b. For example, the $h(\gamma,t)$ at $t = 501$ s, near 10 times of the evaluated longest relaxation time $\tau_{\eta''}$, almost exactly overlapped the $h(\gamma,t)$ at $t = 3$ s at low strains, but was shifted upward at high strains. A similar shifting was observed in 2GDSPBD G(14,12) (see e.g., the $h(\gamma,t)$ at $t = 251$ s), but the deviations from the Doi−Edwards damping were not large even at large strains. The observed upward shifting of $h(\gamma,t)$ at very long times qualitatively implies that the relaxation modulus $G(\gamma,t)$ builds up again at very long time after the imposition of deformation. Similar shifted damping functions were reported for entangled polybutadiene solutions[28] but the physical origins of upward shifting are not known. One possible but simple source is low torque signals at very long times, which may mislead the corresponding properties. The other possible source is the effect of the advected orientation[2,3] by the withdrawal motion, but its surviving time might be too short to build up the relaxation modulus at long times.

Turning to the case of third generation dendritic topology, the corresponding $h(\gamma,t)$ of 3GDSPBD G(5,6,5) exhibited a strong stretching effect well above the Doi−Edwards damping at all times and all strains, as shown in Figure 6c, despite of the approximate time-strain separability. This damping behavior of 3GDS is quite different from that of 2GDS which shows a characteristic damping transition at high strains. In order to examine any effect of the relatively faster longest relaxation time of 3GDSPBD G(5,6,5), the relaxation modulus of linear polybutadiene solutions (PBD L650K10) with a similar longest relaxation time $\tau_{\eta''} = 2.5$ s was also measured. PBD L650K10 was prepared by blending 10 wt % of long linear polybutadiene polymers (L650K, $M_n = 650$ kg/mol) with 90 wt % of short linear polybutadiene chains ($M_n = 5$ kg/mol)). The effective number of entanglements per L650K chain is around 17. As expected, the damping function of the moderately entangled linear polymer solution follows the Doi−Edwards damping function indicating the relaxation moduli $G(\gamma,t)$ of these two samples were properly measured. Also Figure 6d shows the overlapped dynamic moduli $G'(\omega)$ and $G''(\omega)$ of 3GDSPBD G(5,6,5) and PBD L650K10 before and after the step-strain experiments, suggesting the strong stretching effect observed in $h(\gamma,t)$ of 3GDSPBD G(5,6,5) was real. One question this raises is why branch-point withdrawal motion does not appear in this third generation dendritic topology. If withdrawal motion at the middle arm was well separated from that at the inner arm, two separate damping transitions would be expected. On the other hand, if two withdrawal motions occurred consecutively due to the nature of dendritic topology, the damping transition might have appeared at a much larger strain than the theoretical strain in 2GDS and so beyond the accessible experimental window. If the outward thermal force exerted by four outer arms is considered, the theoretical estimate of the strain at which the withdrawal motion of 3GDSPBD G(5,6,5) would occur is at either $\gamma > 27$ for $a_D = a_0/(\phi_{chem})^{\alpha/2}$ or $\gamma > 7.5$ for $a_D = a_0$. The theoretical critical strains become quite broad because the dilution effect increases dramatically in third generation dendritic topology. The effect of multiple branching generations like coupling between different generations is not yet known.[3] Current experimental results, however, suggest that the effect of chain stretching increases with increasing branching generation even though the size of each arm at each generation is only around three entanglement lengths.

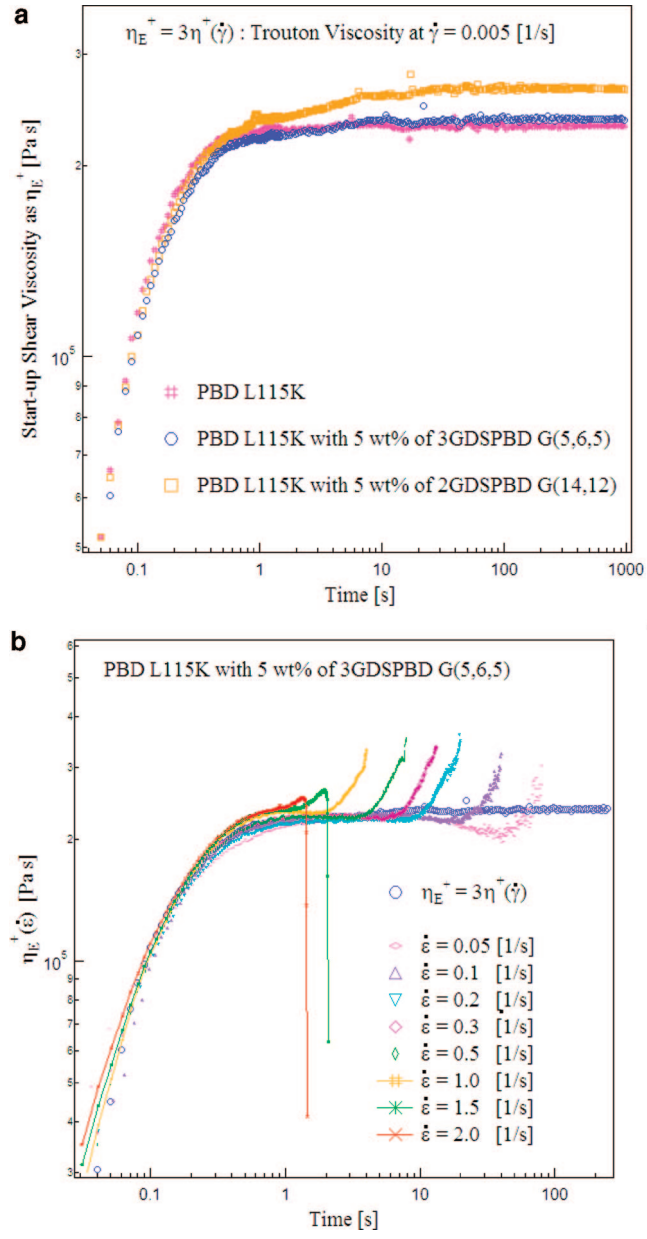

Figure 7. (a) Time-dependent shear viscosities of linear polybutadieme melt (PBD 115K) and the same linear matrix with 5 wt % of second and third generation dendritic star polymers measured at a shear rate $\dot{\gamma} = 0.005$ s^{-1} in terms of the Trouton viscosity. (b) Time-dependent extensional viscosity of linear polybutadiene matrix (PBD115K) with 5 wt % of 3GDSPBD G(5,6,5) at different Hencky rates $\dot{\varepsilon}$.

In order to provide insight into which architecture is most effective in increasing the melt strength without damaging shear properties, the transient extensional viscosity of monodisperse linear polybutadiene polymers (PBD L115K, $M_n = 115$ kg/mol) with 5 wt % of 3GDSPBD G(5,6,5) was measured using a Sentmanat Extensional Rheometer (SER) attached to the MCR 501 at room temperatures (23.5∼25.2 °C). Here, samples were prepared with a stainless-steel plate with 12 mm in width and 0.7 mm in thickness at room temperature under pressure. It is empirically known that the addition of a small amount of branched polymers creates extensional hardening behavior due to the chain stretching effect.[2] Measured damping behavior clearly confirms the stretching effect in these dendritic polymers as either the branch-point withdrawal motion or a strong type B behavior, so extensional hardening was expected by adding dendritic star polymers into linear polymer matrix PBD L115K. Figure 7a show time-dependent shear viscosities of the same

linear matrix with 5 wt % of second and third generation dendritic star polymers measured at a shear rate $\dot{\gamma} = 0.005\ s^{-1}$ in terms of the Trouton viscosity. Addition of 2GDSPBD G(14,12) increased the time-dependent shear viscosity of PBD L115K, while adding 3GDSPBD G(5,6,5) barely changed the shear viscosity of the same linear matrix. It is evident the shear viscosity of a linear matrix increases by adding polymers with higher molecular weights or longer terminal relaxation times. However, the extensional viscosity in Figure 7b indicates the addition of 3GDSPBD G(5,6,5) improved the melt strength of PBD L115K, exhibiting extensional hardening at low Hencky rates but rupturing at high Hencky rates. Of course, the addition of 2GDSPBD G(14,12) will also show such extensional hardening but will increase the shear viscosity more. Therefore, the ideal flow properties in a commercial film blowing process (i.e. shear thinning in extruders and extensional hardening during film formation) may be achieved by designing architectures to have multiple generations with arms of only a few entanglements at each generation. Also this result qualitatively indicates the extensional hardening indeed comes from the effect of architecture (i.e. the degree of chain stretching).

4. Conclusion

We have studied stress relaxation dynamics of a series of well defined second and third generation dendritic star polyisoprene and polybutadiene melts under small-amplitude oscillatory shear as well as nonlinear step shear deformations. Current experimental data provide rheological characteristics belonging to dendritic star polymers, which could be clues to differentiate dendritic topology from other branched architectures. Our findings from measured linear viscoelastic responses indicate the observed tan(δ) minima agree with the expected relaxation hierarchy in dendritic topology. Also the continuously overlapped $G''(\omega)$ at high frequencies provides a hint of relative sizes of outermost arms in second and third generation dendritic architectures. However, the degree of dilution estimated from the ratio of the second plateau modulus to the rubbery plateau modulus suggests a relatively slower rate of dilution due to multiple arms and generations in contrast to the expected ideal self-dilution condition from the dendritic topology where intrachain entanglements seem more plausible than interchain entanglements.

Stress relaxation behavior after the imposition of step shear deformations of well-defined dendritic topology provides clues into rheological features of specific structural units composing the given architectures. A damping function, defined as the ratio of nonlinear relaxation modulus to the equilibrium relaxation modulus measured at very small strains, is a simple measure of the degree of chain stretching. At short times and small strains, the damping behavior of second generation dendritic star polyisoprene and polybutadiene exhibited the chain stretching effect as type B damping above the Doi−Edwards damping function. However, at large strains, the corresponding damping function suddenly followed the Doi−Edwards damping function indicating the branch-point withdrawal motion occurred in these dendritic architectures. Therefore the damping transition from type B to the Doi−Edwards damping is a rheological characteristic not only of H-shaped or multiarm architectures, but also of second generation dendritic star architectures. These architectures commonly contain symmetric Y-shaped structural units where the branch-point withdrawal motion occurs as a sudden retraction at large strains. In the case of third generation dendritic star polymers with arms of a few entanglements at each generation, the corresponding damping function exhibits a strong stretching effect at all strains well above the Doi−Edwards damping function. The expected withdrawal motion was not observed in the accessible experimental window up to a strain of 1500%. However. the measured damping behavior suggests the degree of chain stretching increases with increasing the branching generation. Also the transient shear and extensional viscosities of the linear matrix with 5 wt % of 3GDSPBD G(5,6,5) provides an insight about how to design the branched architecture to improve the melt strength without seriously increasing the shear viscosity.

References and Notes

(1) Milner, S. T.; McLeish, T. C. B. *Macromolecules* **1997**, *30*, 2159.
(2) McLeish, T. C. B.; et al. *Macromolecules* **1999**, *32*, 6738.
(3) Blackwell, R. J.; Harlen, O. G.; McLeish, T. C. B. *Macromolecules* **2001**, *34*, 2579.
(4) Daniels, D. R.; McLeish, T. C. B.; Crosby, B. J.; Young, R. N.; Fernyhough, C. M. *Macromolecules* **2001**, *34*, 7025.
(5) Frischknecht, A. L.; Milner, S. T.; Pryke, A.; Young, R. N.; Hawkins, R.; McLeish, T. C. B. *Macromolecules* **2002**, *35*, 4801.
(6) Juliani; Archer, L. A. *Macromolecules* **2002**, *35*, 10048.
(7) Kapnistos, M.; Vlassopoulos, D.; Roovers, J.; Leal, L. G. *Macromolecules* **2005**, *38*, 7852.
(8) Lee, J. H.; Fetters, L. J.; Archer, L. A. *Macromolecules* **2005**, *38*, 10763.
(9) Kapnistos, M.; Koutalas, G.; Hadjichristidis, N.; Roovers, J.; Lohse, D. J.; Vlassopoulos, D. *Rheol. Acta* **2006**, *46*, 273.
(10) Inkson, N. J.; Graham, R. S.; McLeish, T. C. B.; Groves, D. J.; Fernyhough, C. M. *Macromolecules* **2006**, *39*, 4217.
(11) van Ruymbeke, E.; Bailly, C.; Keunings, R.; Vlassopoulos, D. *Macromolecules* **2006**, *39*, 6248.
(12) van Ruymbeke, E.; Orfanou, K.; Kapnistos, M.; Iatrou, H.; Pitsikalis, M.; Hadjichristidis, N.; Lohse, D. J.; Vlassopoulos, D. *Macromolecules* **2007**, *40*, 5941.
(13) Orfanou, K.; Iatrou, H.; Lohse, D. J.; Hadjichristidis, N. *Macromolecules* **2006**, *39*, 4361.
(14) Doi, M.; Edward, S. F. *The Theory of Polymer Dynamics*; Oxford University Press: New York, 1986.
(15) Osaki, K. *Rheol. Acta* **1993**, *32*, 429.
(16) McLeish, T. C. B. *Macromolecules* **1988**, *21*, 1062.
(17) Bick, D. K.; McLeish, T. C. B. *Phys. Rev. Lett.* **1996**, *76*, 2587.
(18) Archer, L. A.; Varshney, S. K. *Macromolecules* **1998**, *31*, 6348.
(19) Archer, L. A.; Juliani. *Macromolecules* **2004**, *37*, 1076.
(20) Wang, S.; Wang, S. Q.; Halasa, A.; Hsu, W. L. *Macromolecules* **2003**, *36*, 5355.
(21) Lee, J. H.; Goldberg, J. M.; Fetters, L. J.; Archer, L. A. *Macromolecules* **2006**, *39*, 6677.
(22) Watanabe, H.; Ishida, S.; Matsumiya, Y.; Inoue, T. *Macromolecules* **2004**, *37*, 6619.
(23) Watanabe, H.; Sawada, T.; Matsumiya, Y. *Macromolecules* **2006**, *39*, 2553.
(24) Qiao, X.; Sawada, T.; Matsumiya, Y.; Watanabe, H. *Macromolecules* **2006**, *39*, 7553.
(25) Watanabe, H.; Matsumiya, Y.; van Ruymbeke, E.; Vlassopoulos, D.; Hadjichristidis, N. *Macromolecules* **2008**, *41*, 6110.
(26) Perny, S.; Allgaier, J.; Cho, D.; Lee, W.; Chang, T. *Macromolecules* **2001**, *34*, 5408.
(27) Chambon, P.; Fernyhough, C. M.; Im, K.; Chang, T.; Das, C.; Embery, J.; McLeish, T. C. B.; Read, D. J. *Macromolecules* **2008**, *41*, 5869.
(28) Islam, M. T.; Sanchez-Reyes, J.; Archer, L. A. *Rheol. Acta* **2003**, *42*, 191.

MA801429K